Clays and Clay Minerals, Vol. 45, No. 6, 781–788, 1997.

STRUCTURE REFINEMENT OF SYNTHETIC DEUTERATED KAOLINITE BY RIETVELD ANALYSIS USING TIME-OF-FLIGHT NEUTRON POWDER DIFFRACTION DATA

ETSUO AKIBA,[1] HIROSHI HAYAKAWA,[1] SHIGENOBU HAYASHI,[1] RITSURO MIYAWAKI,[2]† SHINJI TOMURA,[2] YASUO SHIBASAKI,[2] FUJIO IZUMI,[3] HAJIME ASANO[4] AND TAKASHI KAMIYAMA[4]

[1] National Institute of Materials and Chemical Research, 1-1 Higashi, Tsukuba, Ibaraki, 305 Japan

[2] National Industrial Research Institute of Nagoya, 1-1 Hirate-cho, Kita-ku, Nagoya, 462 Japan

[3] National Institute for Research in Inorganic Materials, 1-1 Namiki, Tsukuba, Ibaraki, 305 Japan

[4] Institute for Materials Science, University of Tsukuba, Tenoudai, Tsukuba, Ibaraki, 305 Japan

Abstract—The crystal structure of synthetic deuterated kaolinite was refined by Rietveld analysis using time-of-flight (TOF) neutron powder diffraction data. For non-hydrogen atoms, *C1* symmetry was assumed. Starting models were tested in which only the direction of ***O-D*** vectors was varied. The constraints were introduced to all Al-O, Si-O and O-D bonds. The refinement adopting the former gives *P1*(*C1*), a = 5.169(1) Å, b = 8.960(2) Å, c = 7.410(2) Å, α = 91.26(2)°, β = 104.99(2)°, γ = 89.93(1)°, R_{wp} = 3.17%, R_I = 5.78% and S = 1.34 with constraints of l(Al-O) = 1.93 ± 0.05 Å, l(Si-O) = 1.62 ± 0.03 Å and l(D-O) = 0.95 ± 0.15 Å. The inner ***O-D*** vector points toward the tetrahedral sheet. All inner-surface ***O-D*** groups form H bonding with basal O atoms in the next kaolinite layers. The results agreed with those obtained from natural kaolinite.

Key Words—Crystal Structure, Kaolinite, Neutron Powder Diffraction, Rietveld Refinement, Synthetic Kaolinite.

INTRODUCTION

Kaolinite is one of the most important raw materials for industries such as ceramics and papers. Its plasticity is probably related to the H bondings between the surface of the kaolinite particle and water molecules on it. Knowledge of the nature of the H bondings in the crystal structure should be helpful for understanding the chemistry of the kaolinite particle surface.

Of course, the crystal structure of kaolinite has been studied extensively for many years. Adams (1983) refined the crystal structure of natural kaolinite (St. Austell kaolinite) using the neutron powder diffraction technique with *C1* symmetry. Young and coworkers (Suitch and Young 1983; Young and Hewat 1988) reported the crystal structure of Keokuk kaolinite by Rietveld analysis using neutron powder diffraction data. Its structure was described on the basis of a space group *P1* and it was reported that the 2 inner ***O-H*** vectors in its unit cell were differently oriented. Bish and von Dreele (1989) determined the atomic coordinates for Keokuk kaolinite by X-ray diffraction (XRD) analysis, except hydrogen atoms. Bish (1993) made a further refinement of the crystal structure using the data of Young and Hewat (1988). The crystal structure refined by Bish (1993) had symmetry *C1* and the inner ***O-H*** vector was almost parallel to the (001) plane.

On the other hand, some of the authors have been investigating the synthesis of high-purity kaolinite as the main component of the high-performance artificial clay for the ceramics industry (Shibasaki et al. 1992). The synthetic kaolinite is moderate- to high-defect kaolinite with a relatively lower Hinckley Index (Plançon et al. 1988 and 1989). It was necessary to characterize the synthetic sample to control the defect by the synthesis.

In the present work, a sample of deuterated kaolinite was obtained, applying the technique of hydrothermal synthesis of kaolinite, and the crystal structure of deuterated synthesized kaolinite was refined to obtain information for further improvement of kaolinite synthesis. The reason for using deuterated kaolinite is that protium (H) has a large, incoherent scattering cross section of 7.99 × 10^3 m^2, and consequently it makes the signal-to-noise ratio in the neutron diffraction pattern high, as can be seen in the structure refinements of natural kaolinite (see Figure 2 of Young and Hewat 1988).

EXPERIMENTAL

Materials

Deuterated kaolinite was prepared by the procedure described previously (Miyawaki et al. 1991) using heavy water (D_2O) instead of distilled water (H_2O). Silica sol and alumina sol (Snowtex-N and Aluminasol-200; Nissan Chemical Industries, Ltd.) were mechanically mixed in a Si:Al ratio of 1:1 and heated at

† Current address: Department of Geology, National Science Museum, 3-23-1, Hyakunin-cho, Shinjuku, Tokyo, 169 Japan.

Table 1. Initial crystal structure models.

Model	z Coordinates of the inner *O–D* vectors (occupancy)			
	O(6^{i}):z	D(1):z	O(6^{ii}):z	D(1^{iii}):z
C1 up	0.3220 (1.0)	0.3530 (1.0)	0.3220	0.3530
C1 down	0.3220 (1.0)	0.2660 (1.0)	0.3220	0.2660
P1 (up-down)	0.3220 (1.0)	0.3530 (1.0)	0.3220	0.2660
Random	0.3220	0.3530 (0.5)† 0.2660 (0.5)†	0.3220 (0.5)††	0.2660 0.3530 (0.5)††

†,††: The *z* coordinates were refined but the sum of the occupancy of each atom was kept at unity.

Symmetry codes: i) $x, y - 1, z$; ii) $x + \frac{1}{2}, y - \frac{1}{2}, z$; iii) $x + \frac{1}{2}, y + \frac{1}{2}, z$.

873 K for 28.8 ks. Then the mixture was crushed and passed through a 70-mesh sieve. Four grams of the mixture and 16 cm^3 of heavy water (Wako Junyaku, >99.75%) were placed in a Teflon pressure vessel with a capacity of 25 cm^3 (San-ai Kagaku Ltd., HU-25) and heated at 493 K for 432 ks in an electric furnace.

X-ray diffraction patterns of deuterated synthetic kaolinite were essentially identical with those prepared using H_2O. However, the XRD pattern of the synthetic kaolinite suggested that profiles of the diffraction peaks were broader than those of a standard sample such as API #9. The kaolinite content in the product was estimated from a weight loss using thermogravimetry and found to be about 90%. This meant that a certain amount of amorphous materials was included in the sample. The degree of deuteration was confirmed by infrared (IR) spectroscopy. Signals due to O-H stretching (3700–3600 cm^{-1}) were very weak, while sharp peaks due to O-D stretching were clearly observed at 2750–2650 cm^{-1}. These results show that deuteration of kaolinite was nearly perfect.

For comparison, we measured XRD data of the low-defect kaolinite (API #9). The Hinckley indices were 0.8 for synthetic kaolinite and 1.5 for API #9.

Neutron and X-ray Powder Diffraction Measurements

Neutron powder diffraction data were measured on a TOF powder diffractometer, HRP (Watanabe et al. 1987), at the neutron facility (KENS) at the National Laboratory for High Energy Physics (KEK). The sample was placed in a cylindrical vanadium container 10 mm in diameter and 25 μm in thickness. The diffraction angle was fixed at 170°, and the gate width was set at 4–16 μs, depending on TOF. The diffraction data were collected at room temperature for about 43 ks. The computer program RIETAN, which was developed by one of the authors, was used for X-ray and neutron Rietveld analysis (Izumi 1993). Interatomic distances and bond angles were calculated using DAPH (Sakurai 1967) from structural parameters obtained by RIETAN.

X-ray powder diffraction data were obtained at room temperature using a Rigaku RAD-A diffractometer with Cu*K*α radiation. Preferred orientation was reduced using the method reported by McMurdie et al. (1986) for X-ray measurements. The results of Rietveld analysis with and without introducing preferred orientation parameters were essentially identical for both the X-ray and neutron data, which suggests that preferred orientation can be ignored.

Table 2. Metal-oxygen bond lengths and *R* factors before introducing constraints.

Si(1)-O	1.55(6), 1.79(4), 1.65(6), 1.69(5) Å
Si(2)-O	1.87(5), 1.66(4), 1.60(5), 1.57(6) Å
Al(1)-O	1.84(7), 1.81(7), 2.47(6), 1.90(6), 1.64(7), 1.69(6) Å
Al(2)-O	1.38(7), 1.73(6), 2.18(6), 2.08(6), 2.19(6), 2.39(7) Å

R_{wp} = 2.54% ($S = R_{wp}/R_e$ = 1.07), R_p = 1.99%, R_I = 2.83%, R_F = 2.33%.

Table 3. *R* factors obtained with different distance constraints.

l(Al-O)	R_{wp}	R_p	*S*	R_I	R_F
1.89 ± 0.05 Å	3.17%	2.48%	1.34	5.92%	4.37%
1.91 ± 0.05 Å	3.16%	2.48%	1.33	5.83%	4.27%
1.93 ± 0.05 Å	3.12%	2.49%	1.32	5.11%	3.28%
1.95 ± 0.05 Å	3.20%	2.53%	1.35	5.95%	4.58%
1.97 ± 0.05 Å	3.25%	2.57%	1.37	6.15%	4.84%

l(Si-O) = 1.62 ± 0.03 Å, in the *C1 down* model.

l(Si-O)	R_{wp}	R_p	*S*	R_I	R_F
1.60 ± 0.03 Å	3.12%	2.49%	1.32	5.12%	3.29%
1.62 ± 0.03 Å	3.12%	2.49%	1.32	5.11%	3.28%
1.64 ± 0.03 Å	3.11%	2.48%	1.32	5.15%	3.32%

l(Al-O) = 1.93 ± 0.05 Å, in the *C1 down* model.

RESULTS AND DISCUSSION

Rietveld Refinement Using the TOF Neutron Data

Structural models for Rietveld analysis are as follows. The framework composed of Si, Al, O atoms is

Table 4. Metal-oxygen bond lengths and *R* factors by the Rietveld refinement introducing distance constraints for Si-O and Al-O.

Si(1)-O	1.67(3), 1.59(2), 1.65(4), 1.65(4) Å
Si(2)-O	1.67(3), 1.65(2), 1.66(4), 1.65(5) Å
Al(1)-O	1.99(4), 1.87(5), 1.88(5), 1.98(4), 1.88(5), 1.88(4) Å
Al(2)-O	1.98(5), 1.99(5), 1.87(5), 1.96(5), 1.99(4), 1.98(5) Å

R_{wp} = 3.03% ($S = R_{wp}/R_e$ = 1.28), R_p = 2.40%, R_I = 4.13%, R_F = 2.55%.

Constraints: *l*(Al-O) = 1.93 ± 0.05 Å and *l*(Si-O) = 1.62 ± 0.03 Å.

https://doi.org/10.1346/CCMN.1997.0450602 Published online by Cambridge University Press

Table 5. *R* factors obtained by the Rietveld refinement changing hydrogen positions.

Start model	R_{wp}	R_p	S	R_I	R_F
C1 down†	3.27%	2.58%	1.38	6.92%	4.73%
C1 up†	3.33%	2.64%	1.41	6.72%	5.05%
P1(2)†	3.31%	2.66%	1.40	7.32%	5.21%
Random†¶	—	—	—	—	—
2 sites#	2.94%	2.32%	1.25	4.18%	2.83%

† With constraints of l(Al-O) = 1.93 ± 0.05 Å, l(Si-O) = 1.62 ± 0.03 Å and l(D-O) = 0.95 ± 0.15 Å, using the *C1 down*.

¶ Refinement was not converged in this model.

Two positions for the D atom side by side in O(7)-D(2)-O(4) H bondings with constraints of l(Al-O) = 1.93 ± 0.05 Å and l(Si-O) = 1.62 ± 0.03 Å using the *C1 down* model.

Table 6. Interatomic distances and *R* factors obtained by the Rietveld refinement introducing distance constraints for Si-O, Al-O and D-O.

Si(1)-O	1.66(3), 1.66(2), 1.66(5), 1.66(4) Å
Si(2)-O	1.67(3), 1.65(2), 1.66(4), 1.65(5) Å
Al(1)-O	2.00(5), 1.88(5), 1.88(5), 1.99(5), 1.87(5), 1.88(5) Å
Al(2)-O	1.98(6), 1.99(5), 1.93(6), 1.90(5), 1.99(5), 1.88(6) Å
D-O	0.93(6), 0.94(4), 0.90(5), 0.83(5) Å

R_{wp} = 3.17% ($S = R_{wp}/R_e$ = 1.34), R_p = 2.49%, R_I = 5.78%, R_F = 4.07%.

Constraints: l(Al-O) = 1.93 ± 0.05 Å, l(Si-O) = 1.62 ± 0.03 Å and l(D-O) = 0.95 ± 0.15 Å.

assumed to be *C1*, as several authors pointed out (Adams 1983; Suitch and Young 1983; Young and Hewat 1988; Bish and von Dreele 1989; Bish 1993). A starting model for non-hydrogen atoms is that of Bish and von Dreele (1989). Labels for atoms in the present work are identical to those that they described except that the x and y coordinates of Al(2) are $x - ½$ and $y + ½$ of those reported by them and that O(5 + n) and D(n) atoms correspond to O and D atoms of OH(n) groups in their paper. The initial coordinates for the hydrogen atoms were taken from Young and Hewat (1988). Since *R* factors decrease with an increase in the number of refinable parameters without any substantial improvement in Rietveld refinement, we kept the total numbers of refinable parameters in the final refinements within the range of 68–75. In the present work, all occupation factors were fixed at 1.0 and all isotropic thermal parameters at 0.5.

The coordinates of the inner ***O-D*** groups in the present starting models are listed in Table 1. The *C1 up* model has *C1* symmetry, and the inner ***O-D*** vector points toward the octahedral sheet. The inner ***O-D*** vector in the *C1 down* model points away from the octahedral sheet, in other words, toward the tetrahedral sheet. The inner ***O-D*** vector in the *P1* model orients alternatively toward and away from the octahedral sheet. In the random model, inner ***O-D*** vectors randomly orient.

A broad peak due to an amorphous phase was observed in a d range of 3.3–4.7 Å in the XRD patterns. However, only the intensity data between d = 0.8 and 3.3 Å were used in the Rietveld refinements of the TOF data because the intensities of diffraction peaks at d-values larger than 3 Å were weak. Therefore, this broad peak due to the amorphous phase does not affect the analysis of the neutron data. A merit of the TOF diffractometer is that reliable information on reflections with small d-values can be obtained because of the high resolution in the high ***Q*** or low wavelength region. Therefore, it fits the structure refinement of this material.

Table 2 shows the resulting *R* factors and some interatomic distances. As Bish and von Dreele (1989) reported, the obtained distances have a wide range compared with those of dickite (Adams and Hewat 1981; Joswig and Drits 1986) and nacrite (Blount et al. 1969). In order to obtain reasonable distances, nonlinear constraints were imposed on Al-O and Si-O distances (Table 3). On examination of Table 3, we adopted the constraints of l(Al-O) = 1.93 ± 0.05 Å and l(Si-O) = 1.62 ± 0.03 Å.

Table 4 shows the results of Rietveld analysis after introducing the distance constraints. Interatomic distances between D(2) and O atoms are 1.63(4) Å for O(7)-D(2) and 1.63(4) Å for O(4)-D(2). That is, the D(2) atom is located at the middle of the 2 O atoms in the interlayer space. This H position is unrealistic. Therefore, 3 models were introduced for further refinement of H positions. One is a model with a relatively "soft" O-D distance constraint. The second one

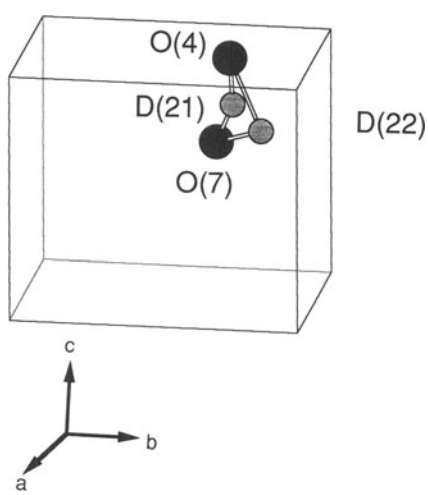

Figure 1. Hydrogen positions refined using the 2 hydrogen sites' model. Interatomic distances are O(4)-D(21): 1.51 Å, O(7)-D(21): 1.50 Å; O(4)-D(22): 2.06 Å and O(7)-D(22): 2.42 Å. Bond angles are O(4)-D(21)-O(7): 151° and O(4)-D(22)-O(7): 81°.

https://doi.org/10.1346/CCMN.1997.0450602 Published online by Cambridge University Press

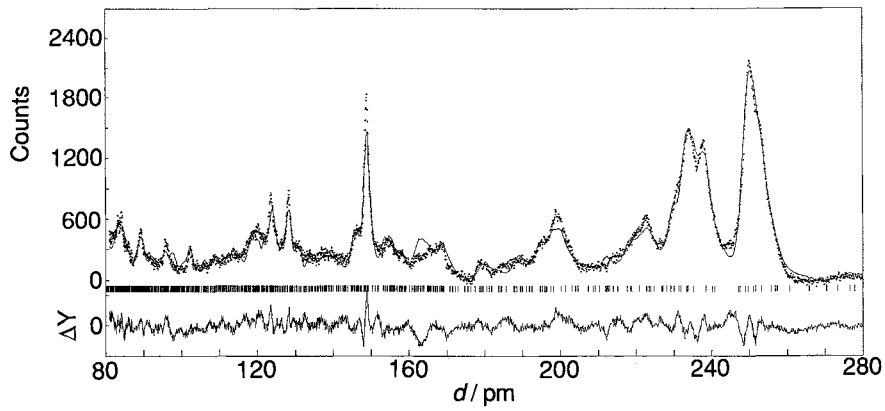

Figure 2. Results of Rietveld analysis for synthetic deuterated kaolinite. Observed and calculated diffraction profiles are shown in dots and the line, respectively. Short bars indicate Bragg angles, and ΔY shows the difference between observed and calculated data.

is a model with 2 H sites side by side between O(7) and O(4). The results of the refinements adopting the 2 models are shown in Tables 5 and 6. Figure 1 shows H positions refined using the 2 H-site models. One H atom, D(21), still locates at the middle of the two O atoms, but another hydrogen, D(22), moves far from the original position. The interatomic distances between the D(22) atom and the neighboring O atoms (O(7) and O(4)) are 2.06 Å and 2.42 Å, respectively. In addition, we put the D(2) atom into 2 sites linearly located between the oxygen O(7) and O(4) atoms as the third model. This can be called the "double minimum hydrogen position model". However, the position of 1 site was almost identical to that in the O-D constraint model, but another site moved far away from the O atoms. Since such results are unrealistic, we did not take 2 H positions for the D(2) site. On the other hand, the results of the refinement with the O-D distance constraint afforded reasonable interatomic distances comparable to those reported for dickite and nacrite (Blount et al. 1969; Adams and Hewat 1981; Joswig and Drits 1986).

Table 7. Crystal structure parameters of deuterated kaolinite. Space group: *P1(C1)*; V = 331.4 Å^3; a = 5.1691(11) Å; b = 8.9595(19) Å; c = 7.4101(18) Å; α = 91.262(16) °; β = 104.98(2) °; γ = 89.928(14) °.

Kaolinite $2(Si_2Al_2O_5(OD)_4)$						
Atom		g†	x	y	z	B††
Al(1)	1a	1.0	0.291(6)	0.521(5)	0.501(4)	0.5
Al(2)	1a	1.0	0.326(8)	0.840(5)	0.507(6)	0.5
Si(1)	1a	1.0	0.984(8)	0.341(2)	0.107(3)	0.5
Si(2)	1a	1.0	0.522(7)	0.164(2)	0.113(3)	0.5
O(1)	1a	1.0	0.063(6)	0.366(4)	0.338(4)	0.5
O(2)	1a	1.0	0.128(7)	0.675(4)	0.345(4)	0.5
O(3)	1a	1.0	0	½	0	0.5
O(4)	1a	1.0	0.206(5)	0.220(4)	0.065(5)	0.5
O(5)	1a	1.0	0.236(4)	0.727(3)	0.001(4)	0.5
O(6)	1a	1.0	0.082(6)	0.996(5)	0.396(4)	0.5
O(7)	1a	1.0	0.012(7)	0.184(4)	0.652(5)	0.5
O(8)	1a	1.0	0.049(6)	0.506(4)	0.649(5)	0.5
O(9)	1a	1.0	0.052(7)	0.885(5)	0.624(5)	0.5
D(1)	1a	1.0	0.152(8)	0.080(3)	0.350(5)	0.5
D(2)	1a	1.0	0.118(6)	0.225(4)	0.794(5)	0.5
D(3)	1a	1.0	0.007(7)	0.526(4)	0.757(4)	0.5
D(4)	1a	1.0	0.073(7)	0.839(4)	0.723(5)	0.5

R_{wp} = 3.17% ($S = R_{wp}/R_e$ = 1.34), R_P = 2.49%, R_I = 5.78%, R_F = 4.07%.

† Occupation factor.

†† Isotropic thermal parameter.

The refinement was carried out by adopting the *C1 down* model.

Constraints were as follows: l(Al-O) = 1.93 ± 0.05 Å, l(Si-O) = 1.62 ± 0.03 Å and l(D-O) = 0.95 ± 0.15 Å.

Labels of non-hydrogen atoms are identical to those reported by Bish and von Dreele (1989) (see text).

Among the models with the distance constraints for Al-O, Si-O and D-O bonds, the *C1 down* model gives the lowest R factors. When the *P1* and *C1 up* models are adopted, inner ***O-D*** vector tends to direct to the tetrahedral sheet like the *C1 down* model with increasing cycle of the refinement. In the *P1* and *C1 up* models, the inner ***O-D*** vector is finally directed to that in the *C1 down* structure, and the atomic coordinates are almost identical to those obtained with the *C1 down* model. The refinement with the random model could not be converged under the same conditions as the other models. Therefore, we conclude that the structure of synthetic deuterated kaolinite has the symmetry *C1* and that the inner ***O-D*** vector is oriented to the tetrahedral sheet. Figure 2 shows the result of Rietveld analysis adopting the *C1 down* model with the constraints for the Al-O, Si-O and D-O distances. Table 7 shows the crystal structure parameters obtained for synthetic deuterated kaolinite using the *C1 down* model. Table 8 lists the interatomic distances and bond angles obtained by the Rietveld method.

The Inner *O-D* Vectors

The direction of the inner ***O-D*** vector(s) is considered to determine the space group of kaolinite. There-

https://doi.org/10.1346/CCMN.1997.0450602 Published online by Cambridge University Press

Table 8. Interatomic distances (Å) and bond angles (°) of synthetic deuterated kaolinite refined with bond-distance contraints for Al-O, Si-O and D-O. Note: Estimated standard deviations in parentheses refer to the last digits. Constraints are as follows l(Al-O) = 1.93 ± 0.05 Å, l(Si-O) = 1.62 ± 0.03 Å and l(D-O) = 0.95 ± 0.15 Å.

Tetrahedral sheet				
			O(1)-O(3)	2.74(3)
Si(1)-O(1^{i})	1.66(3)		O(1)-O(4)	2.64(5)
Si(1)-O(3^{i})	1.66(2)		O(1)-O(5^{iii})	2.88(4)
Si(1)-O(4^{i})	1.66(5)		O(3)-O(4)	2.73(3)
Si(1)-O(5^{ii})	1.66(4)		O(4)-O(5^{iii})	2.35(3)
			O(5^{iii})-O(3)	2.80(3)
Si(2)-O(2^{ii})	1.67(3)		O(2)-O(3)	2.90(3)
Si(2)-O(3^{ii})	1.65(2)		O(2)-O(4^{iv})	2.63(4)
Si(2)-O(4)	1.66(4)		O(2)-O(5)	2.79(5)
Si(2)-O(5^{ii})	1.65(5)		O(5)-O(3)	2.37(3)
			O(3)-O(4^{iv})	2.60(3)
			O(4^{iv})-O(5)	2.90(4)
Octahedral sheet				
Al(1)-O(1)	2.00(5)		O(1)-O(2)	2.79(5)
Al(1)-O(2)	1.88(5)		O(2)-O(6^{ii})	2.79(5)
Al(1)-O(6^{ii})	1.88(5)		O(6^{ii})-O(1)	2.85(5)
Al(1)-O(7^{v})	1.99(5)		O(8)-O(7^{v})	2.87(5)
Al(1)-O(8)	1.87(5)		O(7^{v})-O(9^{ii})	2.69(5)
Al(1)-O(9^{ii})	1.88(5)		O(9^{ii})-O(8)	2.86(5)
			O(1)-O(9^{ii})	2.85(4)
			O(2)-O(8)	2.86(5)
			O(7^{v})-O(6^{ii})	2.61(5)
			O(1)-O(8)	2.62(5)
			O(2)-O(7^{v})	2.60(4)
			O(6)-O(9)	2.02(5)
Al(2)-O(1^{v})	1.98(6)		O(1^{v})-O(2)	2.83(5)
Al(2)-O(2)	1.99(5)		O(2)-O(6)	2.91(6)
Al(2)-O(6)	1.93(6)		O(6)-O(1^{v})	2.87(5)
Al(2)-O(7^{v})	1.90(5)		O(8)-O(7)	2.90(5)
Al(2)-O(8^{v})	1.99(5)		O(7^{v})-O(9)	2.95(5)
Al(2)-O(9)	1.88(6)		O(9)-O(8^{v})	2.75(5)
			O(1)-O(7)	2.94(5)
			O(6)-O(8^{v})	2.65(4)
			O(2)-O(9)	2.86(5)

O-D bonding	O-D distance	D-O distance	O-D-O angle	O..O distance
O(6^{vi})-D(1)-O(4)	0.93(6)	2.55(5)	147(3)	3.39(5)
O(7)-D(2)-O(4^{vii})	0.94(4)	2.16(5)	144(4)	2.97(5)
O(8)-D(3)-O(3^{vii})	0.90(5)	1.83(3)	157(4)	2.68(4)
O(9)-D(4)-O(5^{vii})	0.83(5)	2.27(5)	167(4)	3.09(5)
D(1^{vii})-O(4^{vii})-D(2) angle		147(2)		

Al-Al		Al-Si	
Al(1)-Al(2)	2.87(6)	Al(1)-Si(1^{viii})	3.32(4)
Al(1)-Al(2^{ii})	2.91(6)	Al(2)-Si(1^{iv})	3.27(5)
Al(1^{v})-Al(2)	3.19(6)		
		Al(1)-Si(2^{iv})	3.15(4)
Si-Si		Al(2)-Si(2^{iv})	3.30(5)
Si(1)-Si(2)	2.89(5)		
Si(1^{viii})-Si(2)	3.19(5)		
Si(1)-Si(2^{v})	2.89(3)		

Symmetry codes: i) $x + 1, y, z$; ii) $x + ½, y - ½, z$; iii) $x - ½, y - ½, z$; iv) $x - ½, y + ½, z$; v) $x + ½, y + ½, z$; vi) $x, y - 1, z$; vii) $x, y, z + 1$; viii) $x - 1, y, z$.

fore, the structural studies of kaolinite have placed emphasis on the direction of the inner ***O-D*** vector(s). For example, Adams (1983) reported that the angle between the ***O-D*** vector and the xy plane is 34°, and the ***O-D*** vector directs toward the tetrahedral sheet. He found that the symmetry is *C1*. On the contrary, Young and Hewat (1988) reported that the inner ***O-D*** vectors direct toward the octahedral sheet and the tet-

https://doi.org/10.1346/CCMN.1997.0450602 Published online by Cambridge University Press

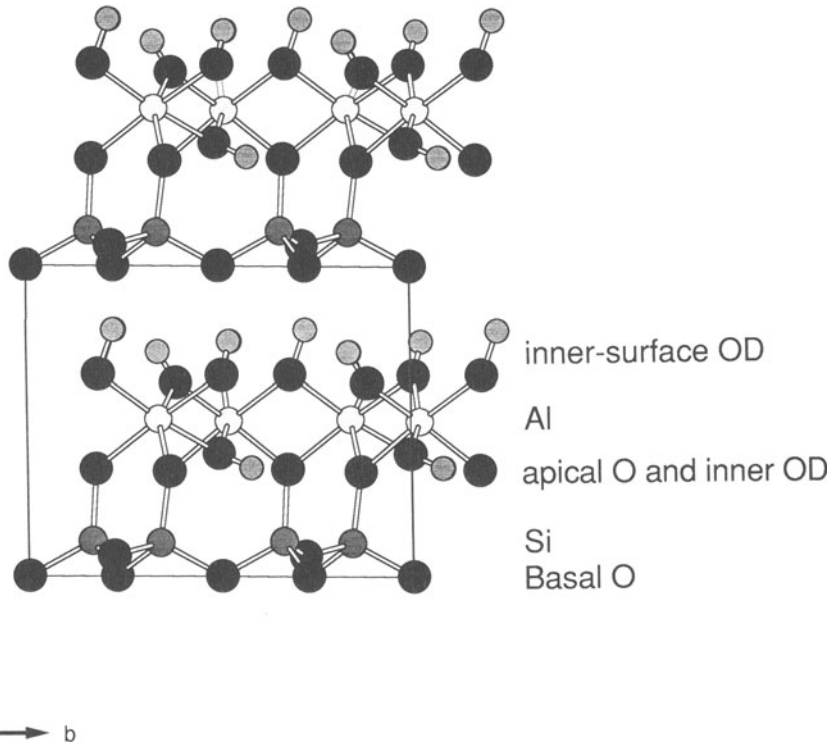

Figure 3. Structure of synthetic deuterated kaolinite viewed along the (100) direction.

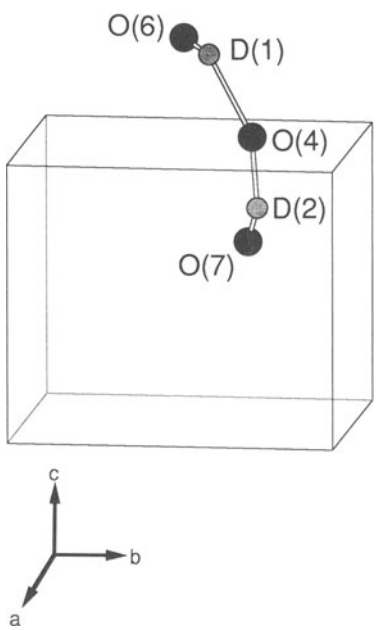

Figure 4. The direction of the inner ***O-D*** vector (projection to the *xy* plane). Basal oxygen, silicon and the inner ***O-D*** vector are shown.

rahedral sheet alternately, and that, therefore, the space group is *P1*. In this work, we find that the inner ***O-D*** vector points toward the tetrahedral sheet and that the angle between the inner ***O-D*** vector and the *xy* plane is 28°. The direction of the inner ***O-D*** vector determined by us is different from the results of Bish (1993), in which the inner ***O-D*** vector is almost parallel to the (001) plane. Figure 3 shows the crystal structure refined in the present work.

The inner D atom, D(1), has several neighboring O atoms such as O(7) (surface O), O(8) (surface O), O(1) (apical O), O(2) (apical O), O(3) (basal O) and O(4) (basal O). Distances from the inner D(1) atom to these O atoms are 2.67(6) Å for O(7), 2.70(5) Å for O(8), 2.59(5) Å for O(1), 2.61(6) Å for O(2), 3.58(5) Å for O(3) and 2.55(5) Å for O(4). The D(1)-O(4) distance is the shortest among them. The projection of the structure for kaolinite on the *xy* plane in Figure 4 clearly indicates that the inner ***O-D*** vector directs toward the basal O(4) oxygen. This suggests formation of a H bond between the inner ***O-D*** vector and basal O(4) atom.

The Inner-Surface ***O-D*** Vectors

The observed interatomic distances of inner-surface O-D bonds are 0.94(4) for O(7)-D(2), 0.90(5) for O(8)-D(3) and 0.83(5) Å for O(9)-D(4). The average distances are slightly shorter than those reported by Bish (1993), but the tendency in the order of distances,

https://doi.org/10.1346/CCMN.1997.0450602 Published online by Cambridge University Press

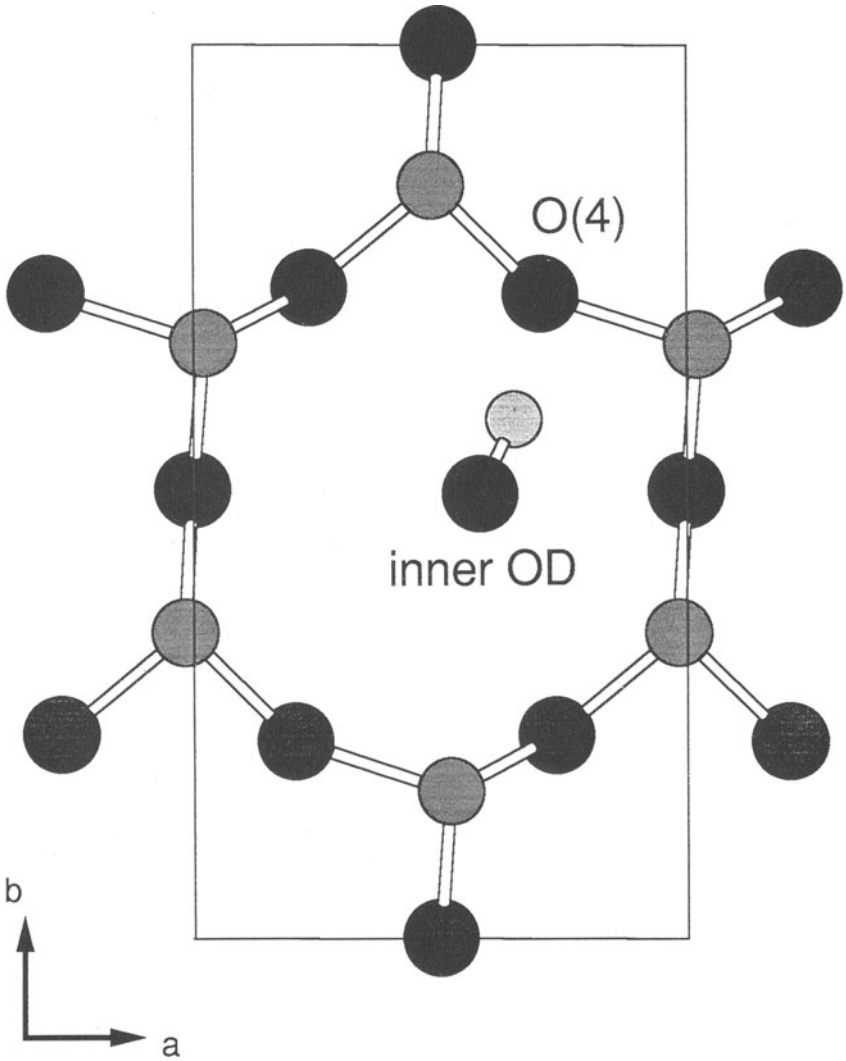

Figure 5. Hydrogen-bond chain in the kaolinite structure.

l(O(7)-D(2)) > l(O(8)-D(3)) > l(O(9)-D(4)), is identical.

The formation of H bonding has been suggested for the inner surface ***O-D*** vectors (Adams 1983; Young and Hewat 1988; Collins and Catlow 1991). The observed interatomic distances in the interlayer are 2.16(5) Å for D(2)-O(4), 1.83(3) Å for D(3)-O(3) and 2.27(5) Å for D(4)-O(5). These H bondings connect the kaolinite sheets and prevent a slip between these sheets. However, the O(7)-D(2)-O(4) H bondings differ from the other 2 H bondings in bond angles. The O(7)-D(2)-O(4) bond angle is 144(4)°, while the O(8)-D(3)-O(3) angle is 158(4)° and the O(9)-D(4)-O(5) angle is 167(4)°. Such variations in the angles of the inner surface ***O-D*** vectors are also described in the reports by Young and Hewat (1988) and by Bish (1993). Bish (1993) explained the difference in the inner-surface ***O-D*** vectors by the assignment of the OH band in infrared spectra.

CONCLUSIONS

Deuterated kaolinite was synthesized using heavy water instead of H_2O. The structure of the deuterated kaolinite has been refined by Rietveld analysis using TOF neutron diffraction data. All the inner ***O-D*** vectors direct toward the tetrahedral sheet and, therefore, the structure of deuterated kaolinite has the symmetry *C1*. The inner surface O-D groups are connected to the basal O of the neighboring kaolinite sheet with H bonding. The results obtained in the present work agree with those obtained from low-defect natural kaolinite.

https://doi.org/10.1346/CCMN.1997.0450602 Published online by Cambridge University Press

ACKNOWLEDGMENTS

The authors thank K. Kuroda of Waseda University for supplying the API #9 kaolinite sample and D. L. Bish of Los Alamos National Laboratory for sending the article before publishing. A part of the present study was supported by the Special Research Program for Important Regional Technology, Agency of Industrial Science and Technology, Ministry of International Trade and Industry, Japan. Two of the authors (E. A. and S. H.) thank the financial support for the present study from Special Coordination Funds of the Science and Technology Agency, Japan.

REFERENCES

Adams JM. 1983. Hydrogen atom positions in kaolinite by neutron profile refinement. Clays Clay Miner 31:352–356.

Adams JM, Hewat AW. 1981. Hydrogen atom positions in dickite. Clays Clay Miner 29:316–319.

Bish DL. 1993. Rietveld refinement of the kaolinite structure at 1.5K. Clays Clay Miner 41:738–744.

Bish DL, von Dreele RB. 1989. Rietveld refinement of non-hydrogen atomic positions in kaolinite. Clays Clay Miner 37:289–296.

Blount AM, Threadgold IM, Bailey SW. 1969. Refinement of the crystal structure of nacrite. Clays Clay Miner 17:185–194.

Collins DR, Catlow CRA. 1991. Energy-minimized hydrogen-atom positions of kaolinite. Acta Crystallogr B47:678–682.

Izumi F. 1993. Rietveld analysis program RIETAN and PREMOS and special application. In: Young RA, editor. The Rietveld method. Oxford: Oxford University Pr. p 232–253.

Joswig W, Drits VA. 1986. The orientation of the hydroxyl groups in dickite by X-ray diffraction. N Jb Miner Mh 1986:19–22.

McMurdie HF, Morris MC, Evans EH, Paretzkin B, Wong-Ng W, Hybbard CR. 1986. Methods of producing standard X-ray diffraction powder patterns. Powder Diffract 1:40–43.

Miyawaki R, Tomura S, Samejima S, Okazaki M, Mizuta H, Maruyama S, Shibasaki Y. 1991. Effects of solution chemistry on the hydrothermal synthesis of kaolinite. Clays Clay Miner 39:498–508.

Plançon A, Giese RF, Snyder R. 1988. The Hinckley index for kaolinite. Clay Miner 23:249–260.

Plançon A, Giese RF, Snyder R, Drits VA, Bookin AS. 1989. Stacking faults in the kaolin-group minerals: Defect structure of kaolinite. Clays Clay Miner 37:203–210.

Sakurai T. 1967. In: Universal crystallographic computation program system (I). Crystallogr Soc Jpn. p 76 [in Japanese].

Shibasaki Y, Tomura S, Miyawaki R, Maeda M, Inukai K, Oda K. 1992. Synthesis technology of kaoliniteic clay. In: Nagasawa K, editor. Proc Workshop WB-1, Clay minerals: Their natural resources and uses; 29th Int Geol Cong; 1992; Nagoya, Japan. p 137–143.

Suitch PR, Young RA. 1983. Atom positions in highly ordered kaolinite. Clays Clay Miner 31:357–366.

Watanabe N, Asano H, Iwasa H, Satoh S, Murata H, Karahashi K, Tomiyoshi S, Izumi F, Inoue K. 1987. High resolution neutron powder diffractometer with a solid methane moderator at pulsed spallation neutron source. Jpn J Appl Phys 26:1164–1169.

Young RA, Hewat AW. 1988. Verification of the triclinic crystal structure of kaolinite. Clays Clay Miner 36:225–232.

(Received 21 February 1994; accepted 15 November 1996; Ms. 2471)